Proneural gene requirements and progenitor dynamics in sensory organ development

Sylvia Dyballa

TESI DOCTORAL UPF / 2015

DIRECTOR DE LA TESI

Dra. Cristina Pujades

BIOLOGIA DEL DESENVOLUPAMENT

DEPARTAMENT DE CIENCES EXPERIMENTALS I DE LA SALUT

upf. Universitat Pompeu Fabra Barcelona

3 RESULTS

Part 1: Identification of the neurosensory progenitor pools

Dora Sapède*, Sylvia Dyballa*, Cristina Pujades.
Cell lineage analysis reveals three different progenitor pools for neurosensory elements in the otic vesicle.
J Neurosc, 32(46):16424-16434, 2012. *Equally contributed

Part 2: Study of the spatiotemporal dynamics of the neurosensory progenitors

Sylvia Dyballa, Thierry Savy, Philipp Germann, Róbert Špir, Mariana Remesikova, Karol Mikula, Andrea Zecca, Nadine Peyriéras and Cristina Pujades.
Cellular dynamics of neurosensory progenitors during embryonic development, to be submitted to Science.

3.1 Identification of the neurosensory progenitor pools

Dora Sapède*, Sylvia Dyballa*, Cristina Pujades. Cell lineage analysis reveals three different progenitor pools for neurosensory elements in the otic vesicle.
J Neurosc, 32(46):16424-16434, 2012. *Equally contributed

Sapède D, Dyballa S, Pujades C. Cell lineage analysis reveals three different progenitor pools for neurosensory elements in the otic vesicle. J Neurosci. 2012 Nov 14;32(46):16424-34. doi: 10.1523/JNEUROSCI.3686-12.2012

3.2 Study of the spatiotemporal dynamics of neurosensory progenitors

Sylvia Dyballa, Thierry Savy, Philipp Germann, Róbert Špir, Mariana Remesikova, Karol Mikula, Andrea Zecca, Nadine Peyriéras and Cristina Pujades Cellular dynamics of neurosensory progenitors during embryonic development, to be submitted to Science.

TITLE

Cellular dynamics of neurosensory progenitors during embryonic development

AUTHORS

Sylvia Dyballa[1], Thierry Savy[2], Philipp Germann[3], Karol Mikula[4], Mariana Remesikova[4], Róbert Špir[4], Andrea Zecca[1], Nadine Peyriéras[2], Cristina Pujades[1]*

AFFILIATIONS

[1]Department of Experimental and Health Sciences, Universitat Pompeu Fabra, PRBB, Barcelona, Spain

[2]Multilevel Dynamics in Morphogenesis Unit, USR3695 CNRS, Gif sur Yvette, France

[3]Systems Biology Program, Center for Genomic Regulation, PRBB, Barcelona, Spain

[4]Department of Mathematics, Slovak University of Technology, Bratislava, Slovakia

*Correspondence to:
Cristina Pujades, PhD
Department of Experimental and Health Sciences
Universitat Pompeu Fabra
PRBB, Dr Aiguader 88,
08003 Barcelona, SPAIN
cristina.pujades@upf.edu
ORCID ID CP: 0000-0001-6423-7451

ONE SENTENCE SUMMARY:
Reconstruction of neurosensory lineages and cellular dynamics during inner ear development

ABSTRACT

Cell lineage follows the normal fate of a cell and its daughters, leading to genealogical trees of cells with increasingly restricted cell fate choices as development proceeds. We have addressed the generation of the lineage tree of the neurosensory elements of the inner ear using a global cell tracing approach. We reconstructed the cell lineage of the otic neurosensory progenitor cells by imaging zebrafish embryos *in vivo* and processing the 3D+time data. We characterized the spatiotemporal pattern of hair cell and neuron generation, and analyze the clonal relationship of the different cell type progenitor pools. Our results demonstrate that the final number of neurosensory progenitors is controlled differently: the number of differentiated hair cells is regulated at the progenitor pool level, meanwhile the final number of sensory neurons is achieved outside the otic epithelium when cells are differentiating within the statoacoustic ganglion.

MAIN TEXT

Two key cell types in the sensory patches underlie the function of the inner ear: the hair cells that transduce the mechanical stimuli, and the sensory afferent neurons, which conduct the extracted information to the brainstem. The generation of a mature functional sensory patch requires a tight coordination between morphogenesis and cell fate specification, to reach the precise number and allocation of these neurosensory elements. These cellular components differentiate very early during embryonic development and arise from the otic ectodermal placode. Gene expression studies showed that neurogenesis and hair cell specification happen simultaneously in zebrafish (*1*), with the neurogenic region partially overlapping with the territories from which sensory patches will develop (*1-5*). The otic epithelium harbors neuronal progenitors, sensory progenitors generating only hair cells, and a pool of progenitors that either give rise to neurons or acquire the hair cell fate (*5-7*). However, how these different progenitor populations are organized within the epithelium and how their relative size changes upon morphogenesis remain still unclear.

In this study, we have explored the dynamic behavior of otic neurosensory progenitors in order to understand the patterning of otic neurosensory cell lineages. We devised a pipeline to extract quantitative biological information from high-resolution 4D image data of developing zebrafish embryos, and captured with single cell resolution the fast dynamic behavior of progenitor cells over long periods of time (14-44hpf; Fig S1), by recording nuclei, plasma membranes and cell fate for the entire system. These data were analyzed using an ad-hoc strategy based in Mov-IT (*8*) to accurately reconstruct the positions, movements and divisions of cells. This allowed us to provide the dynamic map of early neurosensory progenitor pools in the whole organ context. We unveiled that the final number of differentiated hair cells is regulated at the progenitor level, and that sensorigenesis follows a serotyped pattern with first hair cells differentiating at the posterior poles of each maculae and polarizing the structure. In addition, we describe how neuroblast birthdate and position in the otic epithelium prefigure where neurons will be allocated within the statoacoustic ganglion (SAG).

Spatiotemporal development of sensory patches: pattern of hair cell differentiation and map of sensory progenitors

In zebrafish embryos, the anterior (AM, utricular) and posterior (PM, saccular) maculae are the first sensory patches to arise; despite the common mechanisms leading to the formation of sensory cells in both maculae, they develop as two functionally specialized sensory epithelia. To understand their spatiotemporal development, we followed *in vivo* the incorporation of newly differentiated hair cells in the maculae. Tether cells (TC) -the first macular hair cells to differentiate at both ends of the nascent otic vesicle (*9*)- prefigure the position and generate the posterior poles of each maculae (Fig 1A, Mov 1); then the two sensory patches gradually increase in hair cell number, with late-forming hair cells differentiating more dorsally and anteriorly to TC in the AM, or they will be added anteriorly to the TC in the PM (Fig 1A; color-codes correspond to differentiation time). At the end, the AM remains anterior and ventral, and the PM positions medially, next to the ventral edge of the medial wall of the vesicle. Differentiated hair cells never divide and newly differentiated hair cells arise di novo, presumably from the adjacent pool of *atoh1a*-progenitors (Fig S2). This strongly suggests that the final number of differentiated hair cells is regulated by the size and behavior of the progenitor pool. When assessing the kinetics of hair cell differentiation, we observe that AM and PM develop asynchronously: from 25hpf onwards the AM undergoes a progressive and continuous increase in hair cell number, while the onset of differentiation of hair cells in the PM is 2-3h delayed (Fig 1A-B, see AM/PM in control panel; (*4*)).

Previous findings indicated that a pool of neuronal progenitors switch their fate to hair cells of the PM upon abrogation of neurog1 function (*5*). In order to understand the behavior of this progenitor pool, we undertook the same dynamical analysis in morphant embryos for neurog1, which fully recapitulate the phenotype of *neurog1* mutants (*5*), and compared it to the control embryos. In the absence of neurog1 function, otic sensory neurons do not form and supernumerary hair cells are produced in the PM (Fig 1B, (*5*)). Tracking of differentiated cells in time allowed us to compare the dynamics of sensory patch development: the overall spatial pattern of hair cells in the AM/PM is very similar between control and morphant embryos; however the kinetics of hair cell generation in the PM differs due to a boost of hair cell

differentiation from 34hpf onwards (Fig 1B). All supernumerary hair cells arise di novo, with no division of previously differentiated hair cells (Mov 2), suggesting that they originate from recruitment of progenitors allocated anteriorly to the PM, where *atoh1a*-positive cells are (Fig S2).

Next, we sought to generate the spatiotemporal map of hair cell progenitors. Differentiated hair cells were back-tracked to the progenitor state in the context of the whole vesicle, and information about differentiation time and progenitor distribution were combined. The three-dimensional reconstruction of the otic vesicle shows that progenitors for hair cells are located ventrally and medially in the otic vesicle (Fig 1C, control), and the bipotent progenitor pool expands anteriorly and is allocated more medially, as displayed in Fig 1C at different time steps (Mov 3; see map of progenitors at 24hpf). Otic epithelial cells do not rearrange during this period although cells change position due to morphogenetic events, leading to the growth of the PM always towards the anterior and lateral regions (Fig 1C, color-coded cells), meanwhile growth of the AM is mainly anterior and dorsal (data not plotted).

Cell proliferative activity in the sensory/non-sensory domains

The expansion of the bipotent progenitor pool upon downregulation of neurog1 leads to two possibilities: either these progenitors divide more actively, or the pool increases by fast recruitment of adjacent cells to the hair cell fate. To unambiguously respond to this question we analyzed the proliferative activity of the different continuous territories of the otic vesicle (Fig 2). First, we tracked the neighboring cells either located in the dorsolateral region of the otic vesicle (non-sensory domain), or in the ventromedial epithelial domain (sensory domain), during 14h in control embryos. Cell behavior was assessed and cells were color-coded according to the different displayed features (cell division/cell differentiation), meanwhile cell position over time was displayed to achieve spatial organization information attending to proliferative activity (Fig 2A, Mov 4). Cells within the non-sensory domain actively proliferate (see blue cells in Fig 2A) and as expected they do not undergo sensory differentiation (Fig 2A, Mov 4, top row); meanwhile, half of cells located in the ventral region do not divide and undergo hair cell differentiation (Fig 2A, Mov 4, bottom row), supporting the hypothesis that once hair cell progenitors are committed they divide less. To

understand how these different proliferative activities impact the epithelial organization of the whole structure, we measured the cell density of these two domains by assessing the median of the nearest neighbor distance of each territory and plotted these in space and time (Fig 2B). Although cells of the non-sensory domain divide more actively than cells of the sensory domain, the nearest neighbor distance is quite constant in both domains during this time window (Fig 2B, non-sensory domain: from 8μm at 24hpf to 6.5μm from 28hpf onwards; sensory domain: 5μm over all timesteps). Interestingly, eventhough the non-sensory domain displays much higher proliferation activity it is less compacted, suggesting it contributes to the overall growth of the vesicle at this given period. When the same analyses are performed in the MO-neurog1 embryos, similar cell behavior was observed (Fig 2C, Mov 5), confirming that the bipotent progenitor pool does not divide more actively. This suggests that supernumerary hair cells in MO-neurog1 embryos are recruited from an expanded progenitor pool, and supports the hypothesis that the final number of differentiated hair cells relies on the control of the progenitor pool.

Once neuroblasts are specified in the otic epithelium by *neurog1*, they activate *neuroD1* and leave the otic vesicle by a process called delamination (*1*)**.** Upon inhibition of neurog1, no neuroblasts are specified and cells cannot exit the otic epithelium (*2*). Where do the non-delaminated cells allocate within the otic epithelium in the MO-neurog1? We performed an analysis of local cell densities of the entire otic epithelium and plotted the values in the volume of the otic vesicle (Fig 2D, left panel; Mov 6). The global cell density pattern does not change: in both cases, the nearest neighbor distance is smaller in the anteroventral region (Fig 2D, see redish cells in left panel), and extra cells are uniformly allocated within the whole otic vesicle in the morphant. This result suggested that if cell density was not altered but cell numbers were higher (CONTROL n=403cells; MO-neurog1 n=513 cells, see graphs in Fig 4D) the volume of the MO-neurog1 should be about 20% higher than the control vesicle. To test this hypothesis we assessed the whole volume of the otic vesicles by 3D-point-cloud segmentation; as expected, the volume of the MO-neurog1 is about 20% bigger than the control one, with an extra-shoulder in the anteroventral region where many non-delaminating cells allocate (right panel in Fig 2D and Mov 6). Mutants for neurog1 show a similar increase in cell number (Fig S3).

Analysis of the temporal dynamics of neuroblast delamination reveals the posterior expansion of the delamination domain

Sensory neurons derive from neuroblasts that originate in the otic epithelium but delaminate from it to form the SAG close beneath. Clear signs of delamination are first seen at about 16hpf (14 somites), when the ear rudiment is a simple otic placode, although basal blebbing of the epithelial cells even before this suggests that delamination is about to occur (Mov 7; (*1*). The region of delamination, the basal face of the otic epithelium is irregular, with cells straddling what would elsewhere be the line of the basal lamina (Fig 3A, Mov 7). Over the next few hours the number of cells that appear to be delaminating increases, and cells are seen accumulating just below the epithelium (Fig 3C). Delamination starts in the most anterior, ventral and lateral part of the otic epithelium and expands towards the middle of the otic floor to more posterior and medial regions (Fig 3A; (*1*))**.** We segmented the epithelial neuroD-positive domain demonstrating the quick expansion of this territory over time (Fig 3A). Within 1h the delamination domain expands from antero-lateral to posterior-medial (Mov 7). The period of delamination and hair cell differentiation overlap temporally (Fig 4A, Fig 1).

To understand the cell shape changes that neuroblasts undergo upon delamination we have segmented individual delaminating cells. Figure 3B shows an example of a neuroblast passing from the epithelium to the SAG in two axial orientations. The main cell body moves basally in the epithelium in less than 1h (Fig 3B, Mov 8), undergoing apical constriction before exiting the otic epithelium and acquiring properties of migratory cells within the SAG. Analyzing the behavior of several cells by segmentation we observed that neighboring cells behave similarly (Mov 9). Adjacent neuroblasts usually delaminate one after the other from a delamination territory.

As the neuronal precursors delaminate from the otic epithelium they accumulate in the SAG. The rudiment of this ganglion is already clearly seen by 17hpf but the SAG does not become a separate compact mass until 20hpf (Fig 3C, Mov 10). The initial rudiment of the ganglion extends beneath the ventral floor of the vesicle, over an area about one third long in the anterolateral to posteromedial dimension (Fig 3C, dorsal views). There is an intimate relationship between tissue architecture and neuroblast organization within the SAG and ALLg, and it is difficult is to dissociate both events,

since neuroblasts are generated at the same time the otic placode forms (Fig 3C). In some cases it can be observed that cells already specified to be neurons are not fully incorporated in the placode structure (Fig 3C, upper row, early SAG neuroblasts in pink). As early as 20hpf, the SAG rudiment already exhibits capability of innervation to different sensory patches (Mov 11), suggesting that the coarse map of innervation is established very early. This can be observed either in differentiating (neuroD:GFP) and differentiated neurons (Isl3:GFP) (Mov 11).

Position and birthdate of neuroblasts within the otic epithelium prefigure their destination within the SAG

The SAG is composed of two distinct and segregated neuronal populations innervating different sensory patches that appear to express the same molecular signature (*4*). Since this neuronal specificity is established very early (Mov 11), it prompted us to investigate whether neuroblasts were primed to different SAG populations before exiting the otic epithelium. We tracked 190 cells over a period of 12h (Mov 12) and asked: i) what is the neuroblast delamination ratio; ii) do neuroblasts divide before delamination; and iii) is neuroblast identity within the SAG given either by positional and/or temporal information. Figure 4A shows the dynamics of neuroblast delamination with a ratio of 168 delaminating cells over 12h. In the analyzed time window half of delaminating cells do divide before exiting the epithelium, and half after delamination, suggesting that the control of the final number of sensory neurons does not rely on the number of otic epithelial progenitors (see the lineage of neuroblast divisions in Fig S4), and that cell division does not trigger delamination as in other systems (□). How are the posterior and anterior SAG generated? The position of epithelial neuroblasts along the antero-posterior axis defines their position within the SAG: cells found in the anterior portion of the SAG at 30hpf, are specified in the anteromedial floor of the otic vesicle while cells of the posterior SAG come from the posteromedial otic epithelium (Fig 4B upper row; Mov 13). We observe a strong correlation between AP-position of neuroblasts in the epithelium and their AP positioning in the SAG. (Fig 4B middle row; Mov 13). No such correlation was observed regarding the mediolateral axis. (Fig 4B, bottom row; Mov 13). On the other hand, temporal analysis of neuroblast delamination reveals that the mediolateral position of

the neurons in the SAG relies on their delamination order; neuroblasts that delaminate first are allocated more medially in the SAG than those delaminating late (Fig 4C; Mov 14). In further steps of development, the SAG will shift dorsally such that this medio-lateral organization is converted to a dorso-ventral one. As the ear enlarges and the spaces within the head become filled with connective tissue, the ganglion becomes squeezed into the space between the ventromedial wall of the ear and the ventral part of the neural tube (Mov 15). These findings demonstrate that neuronal identity within the SAG is provided by the combination of spatial (anteroposterior) and temporal cues. The fact that we have reconstructed the lineage of the neuroblasts giving rise to the SAG allows us to compare the position of these cells with markers for neuronal specification (Fig S5). As shown in Fig 4D, the neuronal progenitor domain at 18hpf is very wide and expands almost all along the AP axis of the otic placode. A significant amount of cells delaminates in a rather short time window (168 cells in 12h). If the precursors divide before delamination the divisions are mainly symmetric and both daughter cells commit to the neuronal fate. In a few cases at the border of the delamination domain, only one daughter can be observed to delaminate during the analyzed time window; later on, the growth of the structure and the morphogenetic events restrict the delamination domain to a more medial region of the floor of the otic vesicle. The comparison of progenitor maps for hair cells and neurons reveal that progenitor pools for neurons and hair cells are mainly segregated; however, there is a region of possible overlap of progenitors (Fig 4D, Mov 15), which may harbor a progenitor pool able to give rise to both cell fates upon different conditions.

REFERENCES

1. C. Haddon, J. lewis, Early ear development in the embryo of the zebrafish, Danio rerio. *J. Comp. Neurol.* **365**, 113–128 (1996).

2. P. Andermann, J. Ungos, D. W. Raible, Neurogenin1 Defines Zebrafish Cranial Sensory Ganglia Precursors. *Developmental Biology* **251**, 45–58 (2002).

3. B. B. Millimaki, E. M. Sweet, M. S. Dhason, B. B. Riley, Zebrafish atoh1 genes: classic proneural activity in the inner ear and regulation by Fgf and Notch. *Development* **134**, 295–305 (2007).

4. D. Sapède, C. Pujades, Hedgehog signaling governs the development of otic sensory epithelium and its associated innervation in zebrafish. *Journal of Neuroscience* **30**, 3612–3623 (2010).

5. D. Sapède, S. Dyballa, C. Pujades, Cell lineage analysis reveals three different progenitor pools for neurosensory elements in the otic vesicle. *Journal of Neuroscience* **32**, 16424–16434 (2012).

6. T. Satoh, D. M. Fekete, Clonal analysis of the relationships between mechanosensory cells and the neurons that innervate them in the chicken ear. *Development* **132**, 1687–1697 (2005).

7. S. Raft *et al.*, Cross-regulation of Ngn1 and Math1 coordinates the production of neurons and sensory hair cells during inner ear development. *Development* **134**, 4405–4415 (2007).

8. N. Olivier *et al.*, Cell Lineage Reconstruction of Early Zebrafish Embryos Using Label-Free Nonlinear Microscopy. *Science* **329**, 967–971 (2010).

9. B. B. Riley, C. Zhu, C. Janetopoulos, K. J. Aufderheide, A critical period of ear development controlled by distinct populations of ciliated cells in the zebrafish. *Developmental Biology* **191**, 191–201 (1997).

ACKNOWLEDGEMENTS

We are grateful to Thomas Pujol for his valuable help in SPIM imaging, and Zeiss for use of the Lightsheet Z.1 microscope. We thank members of Peyriéras and Pujades laboratories for insightful discussions, especially M Verges and M Linares for technical help. V Lecaudey, A Nechiporuk and B Riley kindly provided transgenic fish lines. SD and AZ were recipients of predoctoral FI-fellowships from AGAUR (Generalitat de Catalunya). This work was supported by the Grant BFU2012-31994, from Spanish Ministry of Economy and Competitiveness (MINECO) and FEDER to CP.

AUTHOR CONTRIBUTION

SD designed the work, performed and analyzed the experiments.
TS provided algorithms in BioEmergences platform.
PG provided the python based framework for quantitative analysis.
KM supervised the segmentation studies.
RS segmented the single delaminating cells.
MK segmented the otic vesicle structure.
AZ was involved in imaging experiments.
NP provided the BioEmergences platform and funding, and analyzed experiments.
CP designed the work, analyzed the experiments, provided funding and wrote the paper.

FIGURE LEGENDS

Figure 1: Spatiotemporal development of sensory patches: pattern of hair cell differentiation and map of sensory progenitors. Differentiated hair cells were tracked during 22h and color-coded according to the differentiation time (see Look Up Table (LUT) in the Figure). A) Stills from Mov 1, showing that first hair cells to differentiate (tether cells) prefigure where the AM and PM will arise, and establish the posterior pole of each maculae; note that differentiated hair cells never divide and the delay in the development of the PM. B) Comparison of the spatiotemporal development of AM/PM in control and MO-neurog1 embryos, showing a similar spatial pattern but a big difference in the temporal pattern of hair cell formation in the PM. Note that supernumerary hair cells in the MO-neurog1 arise *di novo*. C) Map of sensory progenitors for control and MO-neurog1 embryos; differentiated hair cells were back-tracked to the progenitor state. AM/PM, anterior/posterior maculae. Anterior is always to the left.

Figure 2: Cell proliferative activity in the sensory/non-sensory domains. A) Simultaneous tracking of 60 or 50 neighboring cells located in the sensory/non-sensory domains respectively. Centers were color-coded according to cell division and differentiation and plotted on top of the raw data in dorsolateral views at three time steps, or in graphs along time. Transverse section allows the visualization of the position of tracked cells within the dorsoventral axis. Blue, dividing cells; red, non-dividing cells B) Median of the nearest neighbor distance (NN-distance) for the same cohorts of cells than in (A). Lateral vesicle illustrations depict the position and organization of the neighboring cells in the context of the vesicle. Blue LUT, non-sensory cells; green LUT, sensory cells. C) Same analysis than in (A-B), comparing control and MO-neurog1 embryos. Note that there is no difference in NN-distances or proliferative behavior between CONTROL and MO-neurog1. D) Comparison of the NN-distance and local cell densities in the otic vesicle (left side) and otic vesicle volumes (right side) between control and MO-neurog1 embryos. Neither the cell distribution related to the NN-distance nor the pattern of total cell densities change, but the

volume of the MO-neurog1 otic vesicle is larger. Lateral views with dorsal views in inserts. Anterior is always to the left.

Figure 3: Neuroblast delamination domain expands towards posterior over time. Temporal analyses of neuroblast delamination. A) Left panel: Stills from Mov 7 showing how the delamination domain expands from anterolateral to posteromedial within 1h. Right panel: Manual segmentation of the epithelial neuroD-positive cells at three timesteps. Dorsal views with anterior to the left. B) Stills from Mov 8 showing segmentation of a single delaminating neuroblast in transverse (left panel) and lateral (right panel) views, with respective inserts at three timesteps. Note how red cell changes shape and exits the otic epithelium by the basal layer. C) Early organization of neuroblasts within the SAG. Left column displays stills of Mov 10 where tissue architecture and neuroblast delamination are shown simultaneously. Note how at the same time the otic vesicle is forming, neuroblasts are already specified to contribute to two adjacent ganglia, the ALLg and the SAG. Cells are color-coded according to their identity at the given time.

Figure 4: Position and birthdate of neuroblasts within the otic epithelium prefigures their destination within the SAG. A) Cell delamination lineage tree. The lineages of 168 neuroblasts were analyzed for time of delamination. The tree shows the cell lineage from the moment of delamination onwards. Delaminations were grouped in 2h intervals for color-coding (see legend in C). B) Upper row: The two SAG populations were backtracked to their origin in the otic epithelium. Note that cells of the anterior/posterior SAG originate in the anterior/posterior otic epithelium respectively, and they do not intermingle. Middle row: Position of the neuroblasts along the anteroposterior (AP) axis of the otic vesicle foreshadows the relative AP position in the SAG. Note that the french flag AP cell order is maintained from the otic epithelium to the SAG. Bottom row: Position of the neuroblasts along the medilateral (ML) axis of the otic vesicle showing no impact in the relative ML position of cells in the SAG. Note that the Italian flag cell order is not maintained from the otic epithelium to the SAG. C) Delamination order prefigures the position of neuroblasts along the ML axis in the SAG. Note how cells that delaminate earlier are more medially located than cells that

delaminate later. D) Map of neuronal progenitors in the otic epithelium at different embryonic states; sensory neurons in the SAG were backtracked to the progenitor state. Comparison of maps for neuronal and sensory progenitors at 24hpf.

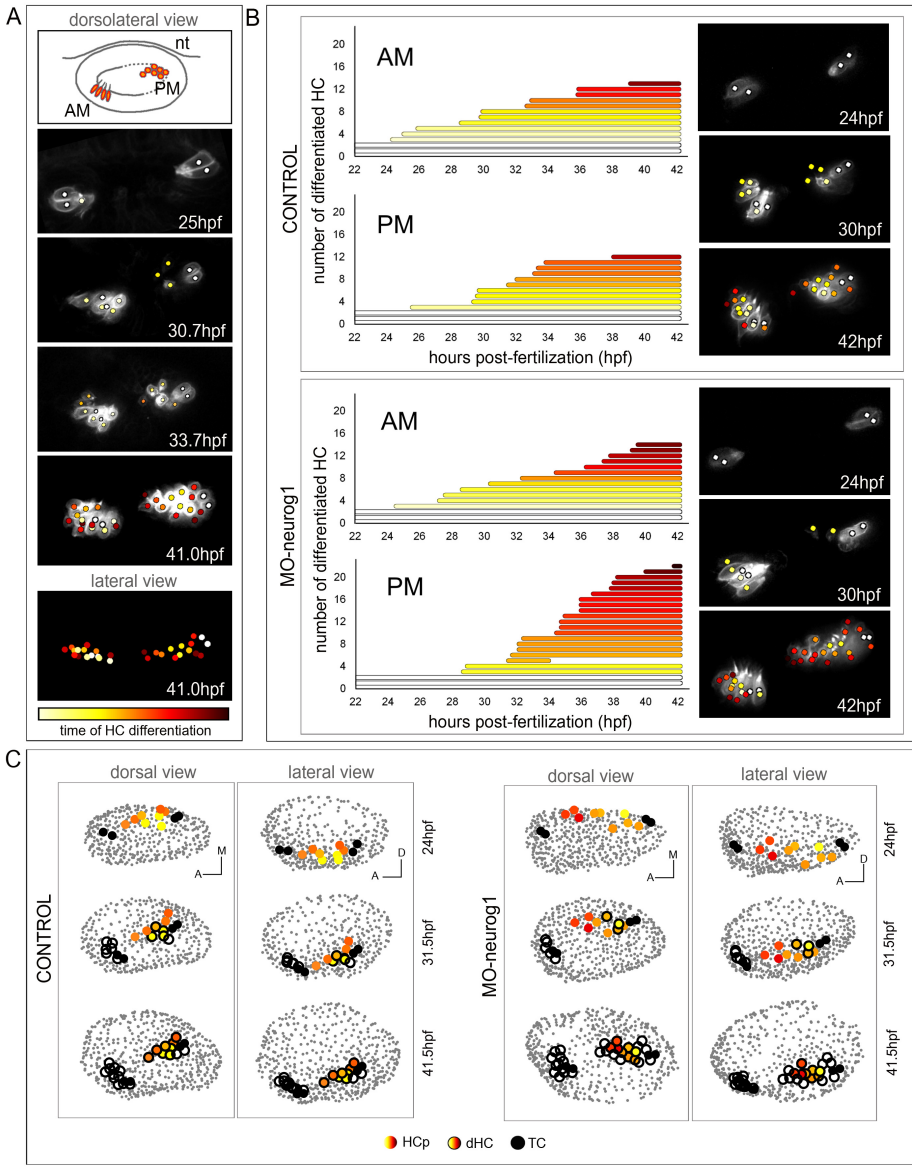

Figure 1: Spatiotemporal development of sensory patches: pattern of hair cell differentiation and map of sensory progenitors.

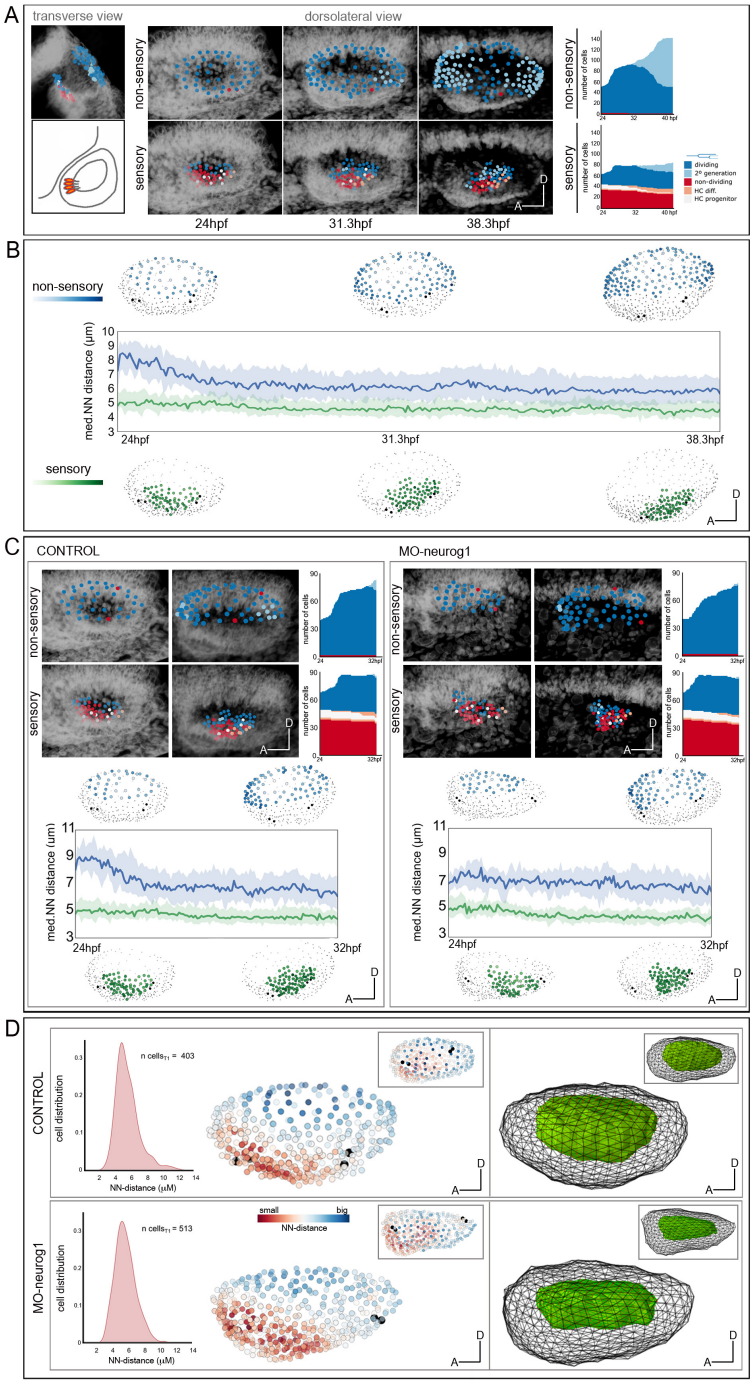

Figure 2: Cell proliferative activity in the sensory/non-sensory domains.

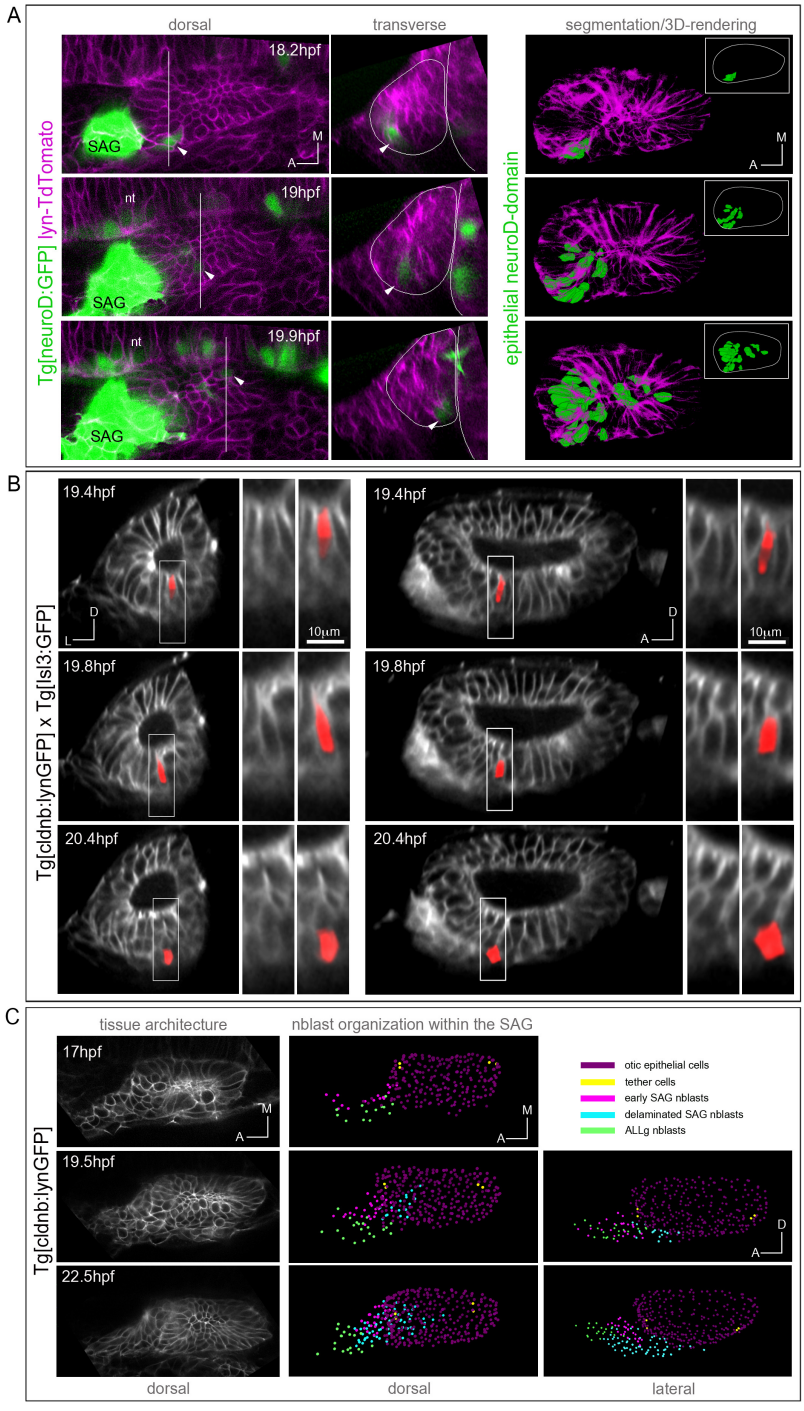

Figure 3: Neuroblast delamination domain expands towards posterior over time.

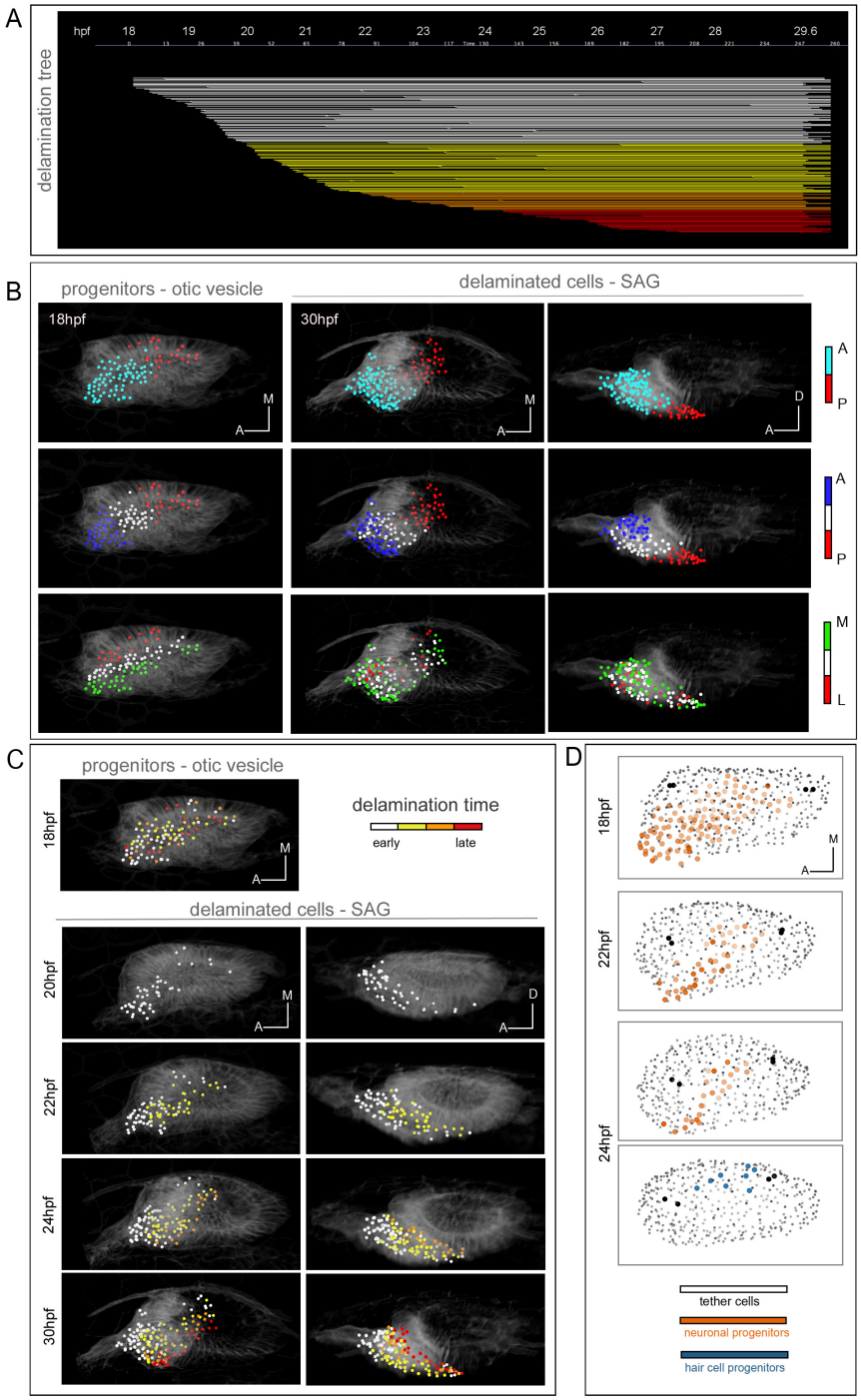

Figure 4: Position and birthdate of neuroblasts within the otic epithelium prefigures their destination within the SAG.

SUPPORTING ON LINE MATERIAL FOR

Cellular dynamics of neurosensory progenitors during embryonic development

Sylvia Dyballa[1], Thierry Savy[2], Philipp Germann[3], Karol Mikula[4], Mariana Remesikova[4], Róbert Špir[4], Andrea Zecca[1], Nadine Peyriéras[2], Cristina Pujades[1]*

[1]Department of Experimental and Health Sciences, Universitat Pompeu Fabra, PRBB, Barcelona, Spain

[2]Multilevel Dynamics in Morphogenesis Unit, USR3695 CNRS, Gif sur Yvette, France

[3]Systems Biology Program, Center for Genomic Regulation, PRBB, Barcelona, Spain

[4]Department of Mathematics, Slovak University of Technology, Bratislava, Slovakia

*Correspondence to:
Cristina Pujades, PhD
Department of Experimental and Health Sciences
Universitat Pompeu Fabra
PRBB, Dr Aiguader 88,
08003 Barcelona, SPAIN
cristina.pujades@upf.edu

SUPPLEMENTARY MATERIALS

MATERIALS AND METHODS

Zebrafish strains

Zebrafish embryos were obtained by mating of adult fish using standard methods. All fish strains were maintained individually as inbred lines. All procedures used have been approved by the institutional animal care and use ethic committee (PRBB–IACUC), and implemented according to national rules and European regulations. Tg[neuroD:GFP] expresses GFP in neuronal progenitors (*1*) and Tg[Isl3:GFP] (also called Isl2b), expresses GFP in the afferent sensory neurons of cranial ganglia (*2*). We generated the Tg[cldnb:lyngfp]Tg[Isl3:GFP] fish line in order to distinguish differentiated and undifferentiated neurons. The Tg[Brn3c:GFP] line expresses GFP in hair cells of the ear and lateral line system (*3*). Tg[cldnb:lyngfp] was previously described in (*4*) and labels the plasma membranes of the otic and anterior lateral line structures. Embryos homozygous for the *neurog1*^{hi1059} mutation (*5*) in the Tg[Brn3c:GFP] background were obtained by incross of heterozygous carriers (*6*); the presence of the *neurog1*^{hi1059} allele was identified by PCR genotyping of tail-clip fins or embryo tails genomic DNA.

In situ hybridization

Whole-mount *in situ* hybridization was carried out as described previously (*7*). Expression of the mRNA was detected with NBT/BCIP substrate. Probes were as follows: *atoh1a* and *atoh1b* (*8*), *neurog1* (*9*), and *neuroD/D4* (*10*).

Antisense morpholinos

For morpholino knockdowns, embryos were injected at 1-cell/stage with translation-blocking morpholino oligomers (MOs) obtained from GeneTools, Inc. neurog1-MO, 5' -ACG ATC TCC ATT GTT GAT AAC CTG G-3' (*11*). Morphants display the same phenotype than *neurog1*^{hi1059} mutants and MO injections were as described in (*6*).

Embryo mounting and SPIM imaging

Embryos were anesthetized in tricaine and mounted in 0.75% LMP-agarose in glass capillaries size 2 (volume 20μl, BRAND GMBH). Imaging was performed on a Zeiss

Lightsheet Z.1 microscope using a 20x or a 40x objective. Imaging was carried out at 26.5ºC and the developmental stage was corrected accordingly (0.7xhpf).

3D+time image analysis pipeline

Preprocessing:

Image pre-processing was done using the Zeiss ZEN software and involved dual (illumination) side fusion and deconvolution (Regularized Inverse Method). In order to compensate for morphogenetic movements semi-automated registration was carried out by using developed FIJI-scripts: The user is guided through the timesteps of the 16-bit .czi data set and chooses by clicking a fixpoint of the structure (eg. a tether cell or a nucleus on the dorsolateral wall of the otic vesicle) for which the x, y, z coordinates are recorded. After navigating through all timesteps of the movie the data set is processed according to the recorded coordinates to generate for each timestep and channel a separate 8-bit Bioemergences VTK file with the corresponding transformation. Furthermore, fluorescent protein bleaching or dilution and changes of transgene fluorescent protein expression levels were compensated by modifying dynamic ranges before 16-bit to 8-bit mapping.

Center detection and automatic tracking:

The generated Bioemergences VTK files were uploaded to the Bioemergences platform (*12*) and center detection was launched. The detected centers were validated using the CenterSelect application (Bioemergences). Subsequently, automatic tracking of the validated centers was launched (EM-Tracking) and once completed the tracking data was validated and curated using the MovIT software and only validated/curated cell tracks were used for further analysis.

Qualitative analysis:

Movies of the developmental processes were generated using FIJI or the MovIT software. For the display of timelapse data the MovIT software has several display modes (Movie 10): raw data can be displayed as orthoslices, volume rendering or oblique slices.

Corrected centers can be grouped in selections and displayed with different appearances alone, or in context of the raw data. Cell lineages can also be displayed as lineage trees. Movies of developmental processes were exported as .tif series and

processed in FIJI. In other cases (Movie 11) the FIJI-3D Viewer was used to generate movies of the volume rendering of image data.

Quantitative analysis:

The centroids of the nuclei were grouped in selections according to states of the cells (eg. dividing or non dividing etc.) and this data was further explored within SciPy, a Python-based ecosystem for scientific computing. Namely the data was imported as Pandas DataFrames; different time points and samples were registered using the iterative closest points transformation algorithm as implemented in Vtk and the results were plotted using matplotlib and seaborn. To estimate the local density, the other centroids within 20μm of each centroid were counted and this number was then divided by the volume of a sphere of that radius. The nearest neighbor distance was used instead when comparing subsets of centroids to limit boundary effects. Both estimates were calculated using *k*-d-trees as implemented in the SciPy library.

Single cell segmentation:

For automatic segmentation of delaminating neuroblasts some cells were chosen in the ventro-medial aspect of the otic vesicle. Additionally to the center that defines the cell lineage of these cells, two more centers were added to each cell to serve as seed points for the segmentation. Automatic segmentation of these cells was then realized by the GSUBSURF method (*13*), which is an image segmentation method based on solving a level set partial differential equation of the form

$$\partial_t u = w_a \nabla g \cdot \nabla u + w_c g |\nabla u| \nabla \cdot \left(\frac{\nabla u}{|\nabla u|}\right),$$

where g is an edge detector function depending on the intensity function of the segmented grayscale image and w_a and w_c are positive real constants steering strength of advective velocity field and curvature regularization. An evolution process of this form converges to a steady state and it is stopped once we do not observe a significant change in the function u. The steady state of evolving level set function u provides a segmentation result which can be directly displayed in FIJI together with the raw data or a selected isosurface of function u can represent the surface of the cell. The equation is solved numerically on image voxel grid by the semi-implicit finite volume scheme and the initial condition is constructed so that we have a reasonable initial

approximation of the segmented cell (e.g. a union of spheres or ellipsoids centered in the provided cell centers).

Segmentation of the otic vesicle structure:

A fully automatic segmentation of the otic vesicle structure would be a rather complicated task – it would not be trivial to construct an appropriate initial condition and to distinguish the borders of the vesicle from the borders of the surrounding cells. Therefore, a different, semi-automatic, strategy was applied. A set of points (usually containing 100-300 points) lying on the surface of the vesicle was marked manually using FIJI; the inner and the outer surfaces were represented by separate point sets. Then we used a method for reconstruction of 3D objects from point clouds described in (*14*). This method is based on Lagrangian evolution of surfaces in 3D and the corresponding evolution model reads

$$\partial_t F = w_a(-\nabla d \cdot N)N + w_c d\Delta F + v_T.$$

Here, we directly evolve the surface represented by the map (parametrization) *F*. The initial condition is an ellipsoid containing the given point cloud in its inside. The function *d* is the distance function to the point cloud and it is the driving force of the evolution. The vector *N* is a unit normal to the surface and *ΔF* is its mean curvature. The parameters w_a and w_c are positive real constants. The vector field v_T is a tangential vector field specifically designed to control the quality of the surface discretization mesh during the evolution. The evolving surface is approximated by a triangulated surface. That means that at the end of the evolution, we directly obtain a triangular representation of the otic vesicle surfaces that can be easily used to compute the volume of the vesicle. As in the case of cell segmentation, the evolution model is discretized semi-implicitly in time and by a finite volume method in space.

Manual segmentation:

Manual segmentation of the delamination domain (as given by neuroD:GFP expressing otic epithelial cells) was done for three timesteps using ITK-Snap. On the other hand the otic vesicle volume was segmented and the resulting vtk file was used to display the membrane signal only of the otic epithelium (FIJI). This domain with the segmented neuroD-positive neuroblasts was displayed using the FIJI-3D viewer.

FIGURE LEGENDS

Figure S1: 3D+time image analysis pipeline.

Embryos were imaged for several hours under a Zeiss Lightsheet Z.1 microscope, and information about plasma membranes, nuclei and cell fate was collected. The acquired data was preprocessed and launched in the BioEmergences platform (http://bioemergences.iscpif.fr) for center detection and automatic tracking. Data was curated and used for: i) qualitative analysis for cell lineages and dynamic behavior studies, ii) automatic segmentation for the analysis of cell morphologies, and iii) quantitative analysis was employed for studies on the tissue architecture. Bottom left depicts the cohort of embryos used in the study.

Figure S2: Spatiotemporal comparison of *atoh1a*-expressing hair cell progenitors with differentiated hair cells.

Tg[Brn3c:GFP] embryos expressing GFP in differentiated hair cells were used for in situ hybridization with atoh1a. Transverse sections at the level of the anterior or posterior maculae.

Figure S3: Total otic vesicle cell numbers at 24hpf of several wild type and neurog1-mutant embryos.

Fixed embryos were used for total cell number analysis. Note that despite small interindividual variations of the total number of cells, an overall increase of 15-20% of the cell numbers is observed in morphants or in mutants for *neurog1*. *neurog1*^{hi1059} mutants are in the Tg[Brnc3:GFP] background.

Figure S4: Cell lineage of neuroblast divisions from 18hpf to 29hpf.

Neuroblasts are tracked within the otic epithelium and the SAG; upon cell division cells are color-coded in red. The branches indicate cells exiting the otic epithelium. Note that approximately 50% of the neuroblasts divide within the otic epithelium and the ones that did not during this period, divide just after delamination. Once delaminated most of the neuroblast population divides within the SAG.

Figure S5: Onset of neuroblast gene expression.

Embryos at 16 and 18hpf were in situ hybridized for *neurog1*, *neuroD1* and *neuroD4*. Note the onset of expression of these genes in the otic vesicle is around 18hpf. Then neuroblasts within the SAG downregulate n*eurog1* and maintain *neuroD1/D4* (*9*, *15*). ALLg/PLLg, anterior/posterior lateral line ganglion; SAg, statoacoustic ganglion; nt, neural tube; oc, otic vesicle.

Movie 1: Spatiotemporal pattern of hair cell generation within the sensory maculae.

Differentiated hair cells were tracked during 22h and color-coded according to the differentiation time (see LUT in the Figure). Upper panel shows color-coded cells on the top of the raw data, and lower panel display only the color-coded cell centers.

Movie 2: Spatiotemporal development of sensory patches in control and MO-neurog1 embryos.

Differentiated hair cells were tracked during 22h and color-coded according to the differentiation time (see LUT in the Figure). Upper row displays orthoslices, middle row displays volume renderings, and lower row displays the cell centers. Note that there are no differences in the spatiotemporal pattern of hair cell generation between the anterior maculae of control and MO-neurog1. Although the spatial pattern of hair cell differentiation does not change in morphant embryos, the temporal pattern is dramatically altered; differentiated hair cells are added to the anterior domain of the PM. AM, anterior macula; PM, posterior macula.

Movie 3: Comparison of the hair cell progenitor pool of the PM of control and MO-neurog1 embryos at 24hpf.

Animation displaying the hair cell progenitor pools (color-coded for time of differentiation) in the context of the whole structure. Note that the hair cell progenitor pools at this stage are ventrally and medially located. In morphant embryos, there is an expansion of the progenitor pool towards anterior and medial.

Movie 4: Cell proliferative activity in the sensory/non-sensory domains.

Simultaneous tracking of 60 or 50 neighboring cells located in the sensory/non-sensory domains respectively from 24hpf to 38hpf. Centers were color-coded according to cell division and differentiation (see legend in the Figure) and plotted on top of the raw data. Transverse view in the left allows the visualization of the position of tracked cells within the dorsoventral axis. Note that many more cells within the non-sensory domain proliferate. Dorsolateral views with anterior to the left.

Movie 5: Comparison of the cell proliferative activity in the sensory/non-sensory domains between control and MO-neurog1 embryos.

Simultaneous tracking of 60 or 50 neighboring cells located in the sensory/non-sensory domains respectively from 24hpf to 32hpf. Centers were color-coded according to cell division and differentiation (see legend in the Figure) and plotted on the top of the raw data. Note that there is no difference in the proliferative activity between control and MO-neurog1 embryos. Dorsolateral views with anterior to the left.

Movie 6: Local cell densities in the otocyst and otic vesicle volumes in control and MO-neurog1 embryos.

Upper panel: Animation showing the overall pattern of total cell densities does not change between control and MO-neurog1 embryos. Note that highest dell density is observed in the anteroventral region (redish cells) in both cases. Tether cells are depicted in black. Lower panel: Animation displaying the otocyst volumes, depicting the basal and apical surfaces of the epithelium. Note the increase in the volume in the case of the MO-neurog1 embryos, corresponding to 15-10% in cell number. Anterior is always to the left.

Movie 7: Expansion of the delamination domain over time.

Movie showing Tg[neuroD:GP] injected with lyn-TdTomato imaged from 14hpf to 22hpf. Upper panel displays only lyn-TdTomato in order to see how tissue architecture undergoes morphogeneis to form the otic vesicle. Middle panel displays neuroD-GFP lyn-TdTomato and neuroblasts are seen within the epithelium and the SAG. Note that the delamination domain expands from anterolateral to posteriomedial within 6h.

Lower panel shows only the neuroD:GFP signal. Note that the SAG rudiment extends a projection towards posterior and innervates the PM. Dorsal views with anterior to the left.

Movie 8: Segmentation of a single delaminating neuroblast in double transgenic embryos Tg[cldnb:GFP]xTg[Isl3:GFP].

Transverse (left panel) and lateral (bottom panel) views with respective inserts. Note that in 1h the red cell changes shape and exits the otic epithelium by the basal layer.

Movie 9: Segmentation of a group of neighboring delaminating neuroblasts in Tg[cldnb:GFP]xTg[Isl3:GFP] embryos.

Transverse (left panel), lateral (middle panel), and dorsal (right panel) views of a group of four neighboring cells. Note that they delaminate very closely in time. Anterior is to the left.

Movie 10: Early organization of neuroblasts within the SAG.

Movie from 17hpf to 23hpf simultaneously displaying tissue architecture and neuroblast delamination. Note how at the same time the otic vesicle is forming, neuroblasts are already specified to contribute to two adjacent ganglia, the ALLg and the SAG. Cells are color-coded according to their identity at the given time. BioEmergences platform allows plotting a projection view with the desired selection of centers, at the same time that provides orthoslices views, oblique view and volume rendering (see right panel).

Movie 11: The coarse map of innervation is established very early.

Movies from 17hpf to 25hpf from Tg[neuroD:GFP] and Tg[Isl3:GFP] embryos showing that as early as 20hpf SAG rudiment already exhibits capability of innervation to different sensory patches. Right panel displays Tg[Brn3:GFP]xTg[Isl3:GFP] embryo at 24hpf demonstrating that at this stage sensory axons from the SAG innervate the PM. Anterior is to the left.

Movie 12: Neuroblasts were followed during 12h.

Transverse view (left panel) and lateral view (right panel) depicting the 194 tracked cells color-coded for cell behavior. See legend in the figure. Anterior is to the left.

Movie 13: Position of neuroblasts within the otic epithelium prefigures their destination within the SAG.

Left panel depicts the information about the overall position of all analyzed cells during this given period (18-30hpf). Note that cells within the otic epithleium at early stages (orange) delaminate (yellow) in order to integrate to the SAG rudiment (blue). Right panel: Top: Neuroblast allocated in the anterior (blue) or in the posterior (red) part of the SAG at 30hpf arise in this very same relative order in the otic epithelium. Middle: Position of the neuroblasts along the anteroposterior (AP) axis of the otic vesicle foreshadows the relative AP position in the SAG. Note that the french flag AP cell order is maintained from the otic epithelium to the SAG. Bottom: Position of the neuroblasts along the medilateral (ML) axis of the otic vesicle showing no impact in the relative ML position of cells in the SAG. Note that the Italian flag cell order is not maintained from the otic epithelium to the SAG. Anterior is to the left.

Movie 14: Neuroblasts delamination date prefigures their destination within the SAG.

Delamination order prefigures the position of neuroblasts along the ML axis in the SAG. Note how cells that delaminate earlier are more medially located than cells that delaminate later (early white, late red). Anterior is to the left.

Movie 15: Maps of hair cell and the neuronal progenitor pool.

Animation displaying the hair cell (blue) and the neuronal (orange) progenitor pools in the context of the whole structure at 24hpf. Note that both progenitor pools are mainly segregated at this stage, although there is a domain where progenitors may be intermingled.

Movie 16: Sensory patches in the embryonic inner ear.

Animation of a double transgenic embryo Tg[Brn3:GFP]xTg[Isl3:GFP] at 48hpf displaying the neurosensory elements. Note that differentiated hair cells of the

maculae are innervated by sensory neurons of the SAG. Anterior to the left and dorsal to the top.

REFERENCES

1. N. Obholzer *et al.*, Vesicular Glutamate Transporter 3 Is Required for Synaptic Transmission in Zebrafish Hair Cells. *Journal of Neuroscience* **28**, 2110–2118 (2008).

2. A. J. Pittman, M.-Y. Law, C.-B. Chien, Pathfinding in a large vertebrate axon tract: isotypic interactions guide retinotectal axons at multiple choice points. *Development* **135**, 2865–2871 (2008).

3. T. Xiao, T. Roeser, W. Staub, H. Baier, A GFP-based genetic screen reveals mutations that disrupt the architecture of the zebrafish retinotectal projection. *Development* **132**, 2955–2967 (2005).

4. P. Haas, D. Gilmour, Chemokine signaling mediates self-organizing tissue migration in the zebrafish lateral line. *Developmental Cell* **10**, 673–680 (2006).

5. G. Golling *et al.*, Insertional mutagenesis in zebrafish rapidly identifies genes essential for early vertebrate development. *Nat Genet* **31**, 135–140 (2002).

6. D. Sapède, S. Dyballa, C. Pujades, Cell lineage analysis reveals three different progenitor pools for neurosensory elements in the otic vesicle. *Journal of Neuroscience* **32**, 16424–16434 (2012).

7. G. Hauptmann, T. Gerster, Two-color whole-mount in situ hybridization to vertebrate and Drosophila embryos. *Trends Genet.* **10**, 266 (1994).

8. B. B. Millimaki, E. M. Sweet, M. S. Dhason, B. B. Riley, Zebrafish atoh1 genes: classic proneural activity in the inner ear and regulation by Fgf and Notch. *Development* **134**, 295–305 (2007).

9. P. Andermann, J. Ungos, D. W. Raible, Neurogenin1 Defines Zebrafish Cranial Sensory Ganglia Precursors. *Developmental Biology* **251**, 45–58 (2002).

10. M. Itoh, A. B. Chitnis, Expression of proneural and neurogenic genes in the zebrafish lateral line primordium correlates with selection of hair cell fate in neuromasts. *Mech. Dev.* **102**, 263–266 (2001).

11. R. A. Cornell, J. S. Eisen, Delta/Notch signaling promotes formation of zebrafish neural crest by repressing Neurogenin 1 function. *Development* **129**, 2639–2648 (2002).

12. N. Olivier *et al.*, Cell Lineage Reconstruction of Early Zebrafish Embryos Using

Label-Free Nonlinear Microscopy. *Science* **329**, 967–971 (2010).

13. K. Mikula, N. Peyriéras, M. Remesikova, O. Stašová, Segmentation of 3D cell membrane images by PDE methods and its applications. *Comput. Biol. Med.* **41**, 326–339 (2011).

14. P. Daniel, M. Medla, K. Mikula, M. Remesikova, Reconstruction of Surfaces from Point Clouds Using a Lagrangian Surface Evolution Model.

15. D. Sapède, C. Pujades, Hedgehog signaling governs the development of otic sensory epithelium and its associated innervation in zebrafish. *Journal of Neuroscience* **30**, 3612–3623 (2010).

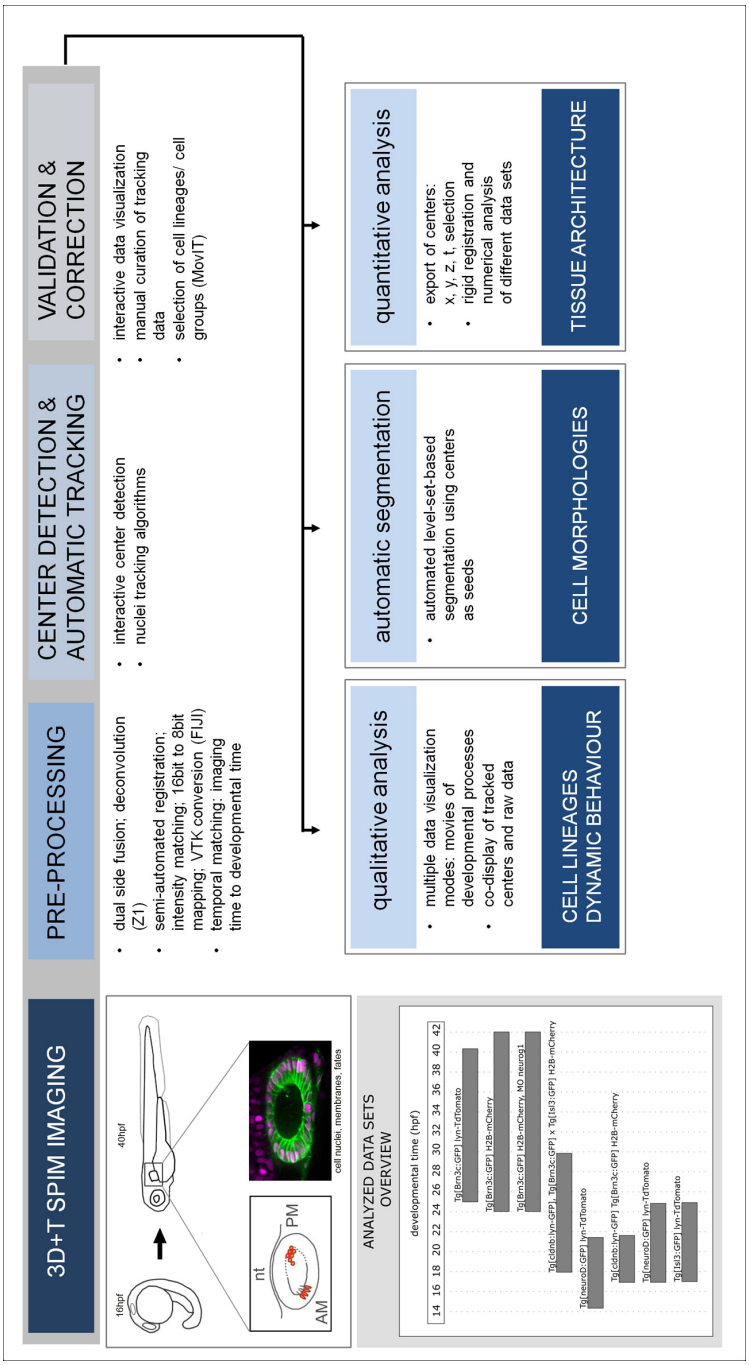

Figure S1: 3D+time image analysis pipeline.

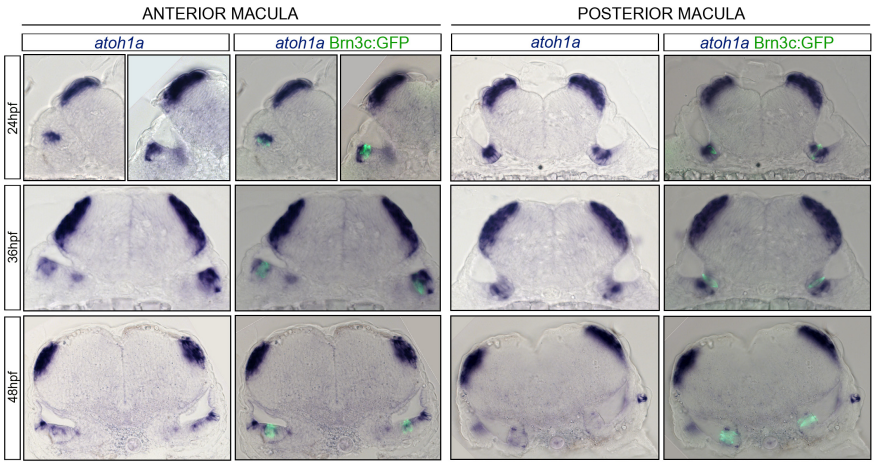

Figure S2: Spatiotemporal comparison of *atoh1a*-expressing hair cell progenitors with differentiated hair cells.

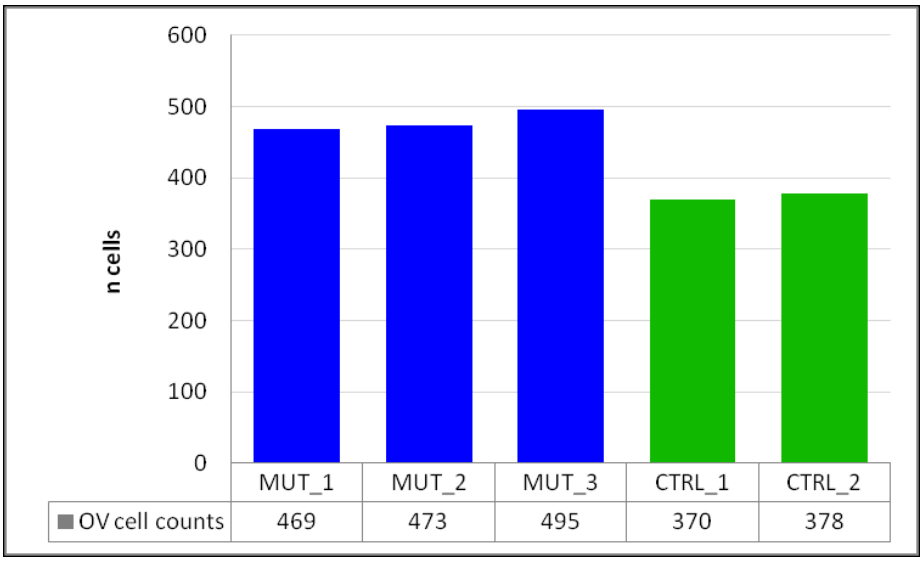

Figure S3: Total otic vesicle cell numbers at 24hpf of several wild type and neurog1-mutant embryos.

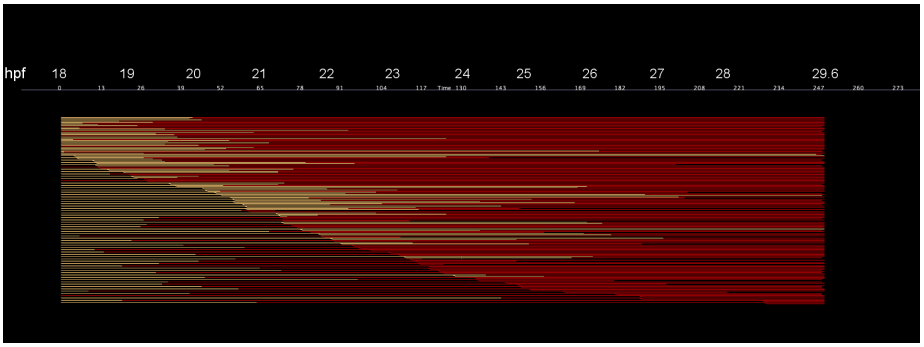

Figure S4: Cell lineage of neuroblast divisions from 18hpf to 29hpf.

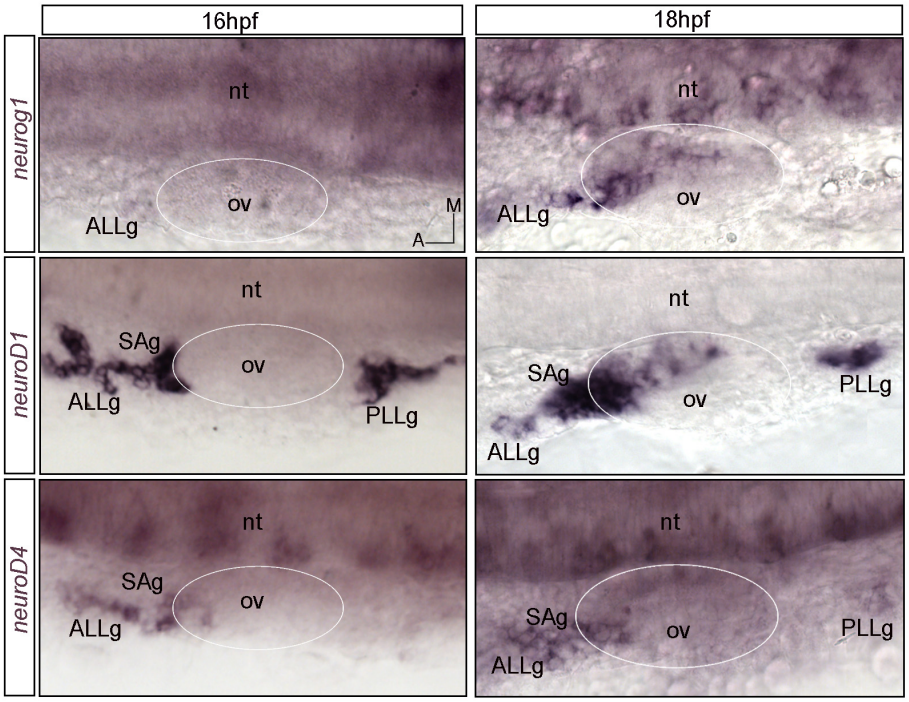

Figure S5: Onset of neuroblast gene expression.